

# Structural resistance of high-strength steel CHS members.



# Structural resistance of high-strength steel CHS members

Aglaia E. Pournara and Spyros A. Karamanos[1]
*University of Thessaly, Volos, Greece*

Elisabetta Mecozzi and Antonio Lucci
*Centro Sviluppo Materiali S.p.A., Rome, Italy*

## ABSTRACT

The structural resistance of high-strength steel seamless tubular beam-columns of circular cross-section subjected to axial compression and bending loading is investigated, using experimental testing and numerical finite element simulations. Experiments on short and slender seamless tubular specimens are conducted, and simulated with rigorous finite element models. Prior to experimental testing, initial imperfections and residual stresses are measured, and the measurements are taken into account in the numerical models as initial conditions. A good comparison is achieved between numerical simulations and experimental results in terms of ultimate strength capacity. Using the finite element tools, parametric numerical analyses are conducted under combined axial-bending loading conditions. First, the influence of initial imperfections (wrinkling) on the structural behaviour of high-strength steel tubular members is examined, in terms of their cross-sectional strength. Subsequently, stability curves for axial compression, and thrust-bending interaction diagrams for the high-strength steel tubular members are obtained. The cross-sectional strength, the stability curves and the interaction diagrams obtained numerically are compared with existing relevant provisions of European and American specifications (EN 1993, API RP 2A and AISC) for the design of beam-column tubular members. The comparison shows that the provisions of those specifications, originally developed for mild steel CHS members, result in reasonable, yet conservative, predictions for the structural resistance of high-strength steel seamless CHS members. It is also suggested that significant improvement of EN 1993 predictions can be achieved revising the classification of high-strength steel CHS sections.

## 1. INTRODUCTION

Tubular CHS members offer reliable and cost-effective structural design solutions because of their excellent structural and architectural properties. They are used as steel building columns or members of lattice structures (masts or towers). In those applications, tubular members are primarily subjected to axial and bending loading, which may result in failure due to structural instabilities i.e. global or local buckling. During the last two decades, high-strength steel CHS members have become commercially competitive and their use in steel construction industry is continuously growing due to the increasing demand for lightweight structural systems with high structural performance. In addition, the use of high-strength steel, with yield strength from 460 to 690 MPa, could provide cost efficient solutions in column and beam-column member design because of increased structural

[1] Corresponding author; email: skara@mie.uth.gr

strength, resulting in structures with high values of strength-to-weight ratio. One should notice that the stress-strain material behavior of high-strength steel is considerably different from that of mild steel, exhibiting significant strain-hardening at lower strain levels, despite its lower overall material ductility. Previous studies on the buckling behavior of high-strength steel structural members (mainly to H, I and box sections) have been reported by Rasmussen and Hancock [1], Beg [2], Sivakumaran and Bing [3], Johansson and Collin [4], Shi *et al*. [5]. These works have indicated that those structural members of H, I or box section have a good structural performance and have also suggested that, as a conservative approach, the existing design rules for mild steel members (e.g. EN 1993-1-1) can be used for the design of high strength steel members.

The existing research work on the ultimate capacity of CHS structural members refer almost exclusively to steel grades up to 460 MPa. Notable experiments on CHS tubulars subjected to bending have been reported in the '70s by Sherman [6] on 10-inch-diameter fabricated tubes with $D/t$ ranging from 18 to 110, and Korol [7] on eleven tubular specimens with $D/t$ between 29 and 80. Chen and Ross [8] have performed axial compression tests on fabricated tubular members with $D/t$ ratio between 48 and 70 and reported residual stress measurements. Prion and Birkemoe [9] performed tests on twenty two 450-mm-diameter tubular specimens subjected to combinations of axial compression and bending, whereas more recently, a series of bending tests on tubular members with $D/t$ ranging from 36 to 120 have reported by Elchalakani *et al*. [10] towards examining existing slenderness limits for CHS sections. The reader is referred to the review papers of Miller [11], Kulak [12] and Dorey *et al*. [13] for an overview and evaluation of numerous test data on tubular CHS members. Furthermore, a significant number of experiments have been performed to determine strength and deformation of steel tubes and pipes, motivated by offshore pipeline applications; bending tests on small-scale scale specimens have been reported by Reddy [14] and Kyriakides and Ju [15], whereas Gresnigt and Van Foeken [16] performed bending tests on four UOE and seamless 20-inch-diameter tubes. In addition to the above tests, analytical investigations on the ultimate capacity of tubular members have been reported by Toma and Chen [17], Sohal and Chen [18], Wagner *et al*. [19], using a simplified analytical methodologies whereas more rigorous results on beam-column behavior have been reported by Karamanos and Tassoulas [20], using a special-purpose numerical technique.

In a series of publications, Zhao and co-workers [21] [22] investigated experimentally the ultimate capacity of CHS members made of very high-strength steel (yield stress equal to 1350 MPa), subjected to compression and bending. These test results indicated that the value of diameter-to-thickness ratio $D/t$ required so that the bending strength of these tubes reaches the yield bending moment and the plastic bending moment values is equal to 48.9 and 36.7 respectively. Furthermore, it was shown that those very high-strength steel tubes with $D/t$ equal to 21 are capable of sustaining a bending curvature larger than four times the curvature at first yield $k_y$. The above $D/t$ values are significantly higher than the ones predicted by the EN 1993-1-1 classification for CHS sections. Despite the fact that the work in [21] [22] refers to CHS members with yield stress equal to 1350

MPa (significantly higher than the steel grade range of interest), the above observations are a clear indication that EN 1993-1-1 provisions on classification penalize the strength of high-strength steel sections, by a substantial amount.

In structural engineering practice, the design of CHS tubular beam-columns under axial compression and bending conditions is covered by the current provisions of EN 1993 standard. In particular, for CHS members of class 1, 2 and 3, the EN 1993-1-1 provisions in sections 6.2 and 6.3 should be used for strength calculations [23], whereas the designer should also employ the provisions of the EN 1993-1-6 standard [24] for calculating the cross-sectional strength of class 4 sections. These provisions in EN 1993 are applicable for steel grade up to 460 MPa. It should be noted that the recent EN 1993-1-12 standard [25] for the use of high strength steel in structural applications does not impose any restriction on the use of EN1993-1-1 design rules for CHS beam-columns made of high-strength steel (up to S700 steel grades). The AISC specification for hollow sections [26] contains rules for structural steel tube design. In addition, the API RP2A specification [27], which refers to the design of fixed offshore steel platforms, is another source of design provisions for tubular CHS members (Chapter D). However, these American specifications do not cover the case of high-strength steel. Moreover, the CIDECT guidelines [28] for the stability of the tubular CHS members have adopted the provisions of European pre-standard ENV 1993-1-1, issued before the launch of EN 1993, and will not be considered in the present study.

In this paper, experimental and numerical work is reported aimed at providing background on the structural behaviour and resistance of CHS high-strength steel beam-columns. In particular, it examines the buckling strength of seamless CHS tubulars made of T590 steel grade, subjected to combined axial and bending loading conditions. The study constitutes a joint research effort of Centro Sviluppo Materiali S.p.A. and the University of Thessaly, is a part of European RFCS project ATTEL [29], and it is aimed at developing structural design guidelines for high-strength steel CHS members and welded tubular connections within the EN 1993 framework. Cross-sectional strength, stability curves under axial compression of slender columns, and interaction diagrams for the combined action of thrust and bending loads are presented. Finally, a critical evaluation of slenderness limits for CHS member classification in EN 1993 is performed, and a comparison is conducted with the buckling provisions for CHS members from three major specifications in Europe and in the U.S.

## 2. EXPERIMENTAL INVESTIGATION

### 2.1 Tubular Specimens

Full-scale experiments have been performed on ten 1.5-meter-long tubular specimens (“short” specimens) and eight 5-meter-long tubular specimens (“long” specimens) summarized in Table 1. The steel tubes are seamless, made of TS590 steel material (nominal yield stress equal to 590 MPa), produced by Tenaris Dalmine S.p.A. Two cross-sections have been chosen for the specimens; the nominal outer diameter $D_{nom}$ and thickness $t$ of the first tubular section, denoted as “A”, are equal to 355.6 mm (14 inches) and 12.5 mm, respectively, while

for the second cross-section, denoted as “B”, the outer diameter is equal to 323.9 mm (12.75 inches) and the thickness equal to 10 mm.

### 2.2 Material Properties

Uniaxial tension tests on coupon strip specimens have been conducted to obtain the real properties of the steel material. The material stress-strain curve is shown in Figure 1, indicating that the values of yield stress $\sigma_y$ and ultimate stress $\sigma_u$ are equal to 723MPa and 802MPa, respectively, significantly higher than the nominal values. Following a small initial “plastic plateau” (a region with very small hardening modulus), significant strain hardening of the material starts at 0.5% engineering strain, reaching an ultimate stress of 802MPa at 7% strain, indicating a rather low ductility, which is typical for high-strength steel, compared with mild steel ductility.

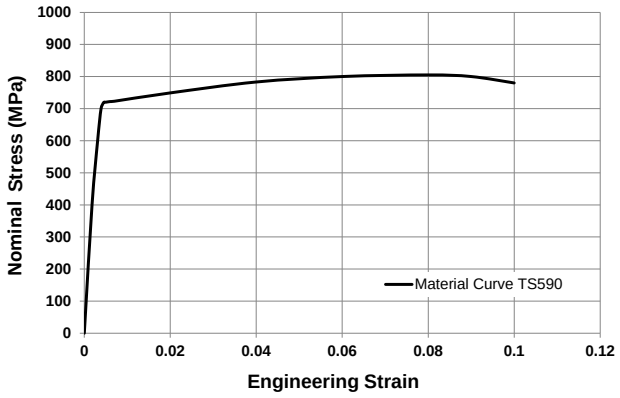


**Figure 1**. Material stress-strain curve of TS590 high-strength steel tubular specimens.

### 2.3 Imperfection and residual stresses measurements

Measurements on thickness variation and initial wrinkling of tube wall have been obtained from the tubular specimens prior to testing. This information is used in the finite element simulations, described in detail in a later section of the present paper. In addition to those geometric measurements, residual stress measurements have been obtained.

Thickness variation is measured at eight equally-spaced points around several cross-sections along the specimen using an ultrasonic device. The mean thickness values are summarized in Table 1 for each specimen. In Table 1, labels AS and BS refer to short tubular specimens of cross-section "A" and "B" respectively, while the AL and BL labels, refer to long specimens with "A" and "B" cross-sections. In AS specimens, thickness values range from 12.1 mm to 13.83 mm, while for BS specimens the thickness varies between 9.80 mm and

11.59 mm. Similarly, the actual thickness values of specimens AL range from 12.08 mm to 13.97 mm, while the thickness of BL specimens varies between 10.08 mm and 11.83 mm [30].

Initial wrinkling measurements have been obtained before experimental testing using special-purpose equipment, shown in Figure 2a. The equipment consisted of a stiff aluminium reference frame, capable of rotating around the reference axis of the column, and is equipped with a sliding guide supporting an LVDT, always in contact with the outer surface profile of the cylindrical member. Each tubular member has been placed on the measuring device, as shown in Figure 2a, and initial wrinkling of the tube wall has been measured at several points along eight equally-spaced generators of the cylinder. The maximum value of wrinkling amplitude is measured equal to 3.62% of tube thickness, as described in detail by Pappa *et al*. [30], which is a rather small value but quite reasonable for seamless tubes.

Residual stresses have also been measured, in the axial and hoop direction. In the hoop direction, the "splitting ring" method has been used according to ASTM E1928-99. Two (2) rings of 18-mm-width each have been extracted from tube specimen of section A, and split as shown in Figure 2b. This resulted in an opening ring size (gap) $g$ equal to 17.7 mm, corresponding to a maximum/minimum hoop stress equal to ±122 MPa (about 17% of the actual yield stress) calculated as follows:

$$S = \pm \frac{t}{2} \frac{E}{\left(1-\nu^2\right)} \left( \frac{R_1 - R_0}{R_0 R_1} \right) \qquad (1)$$

where $E$ is Young's modulus, $t$ is tube thickness, $\nu$ is Poisson's ratio and $R_0, R_1$ are the mean outside radii before and after splitting respectively, which can be readily expressed in terms of gap $g$. The residual stresses in the axial direction have been measured from the curvature of longitudinal strips extracted from the tubular specimens. Using elementary beam-bending theory, this resulted in the calculation of a maximum longitudinal stress equal to 26 MPa, which is only 4% of the yield stress of the tube material [30]. Therefore, the longitudinal residual stresses can be disregarded in the finite element simulation.

### 2.4 Experimental set-up

The specimens are subjected to axial and bending loading, with the use of the testing rig shown in Figure 3 located at CSM Full Scale facilities. This testing device can accommodate tubular specimens of length up to 5 meters, with diameter sizes from 8 to 20 inches. The main actuator can apply a maximum axial force of 25 MN in tension and 30 MN in compression. Furthermore, bending can be applied using the two hydraulic cylinders located on each side of the specimen, with a maximum bending capacity of 3 MNm.

**Table 1**. Mechanical properties and loading pattern of tubular specimens

| Specimens | ID | $D_{nom}$ (mm) | $t_{mean}$ (mm) | $L$ (mm) | Type of Loading |
|---|---|---|---|---|---|
| Short | AS1 | 355.6 | 12.49 | 1490 | Axial |
| | AS-13 | 355.6 | 12.50 | 1850 | Axial 13% → Bending |
| | AS-25 | 355.6 | 12.64 | 1850 | Axial 25% → Bending |
| | AS-50 | 355.6 | 12.79 | 1850 | Axial 50% → Bending |
| | AS-75 | 355.6 | 12.62 | 1850 | Axial 75% → Bending |
| | BS1 | 323.9 | 10.26 | 1490 | Axial |
| | BS-13 | 323.9 | 10.00 | 1850 | Axial 13% → Bending |
| | BS-25 | 323.9 | 10.86 | 1850 | Axial 25% → Bending |
| | BS-50 | 323.9 | 10.86 | 1850 | Axial 50% → Bending |
| | BS-75 | 323.9 | 10.79 | 1850 | Axial 75% → Bending |
| Long | AL1 | 355.6 | 12.74 | 4490 | Axial |
| | AL-25 | 355.6 | 12.78 | 4850 | Axial 25% → Bending |
| | AL-50 | 355.6 | 12.97 | 4850 | Axial 50% → Bending |
| | AL-75 | 355.6 | 12.84 | 4850 | Axial 75% → Bending |
| | BL1 | 323.9 | 10.88 | 4490 | Axial |
| | AL-25 | 323.9 | 10.84 | 4850 | Axial 25% → Bending |
| | AL-50 | 323.9 | 10.82 | 4850 | Axial 50% → Bending |
| | AL-75 | 323.9 | 10.80 | 4850 | Axial 75% → Bending |

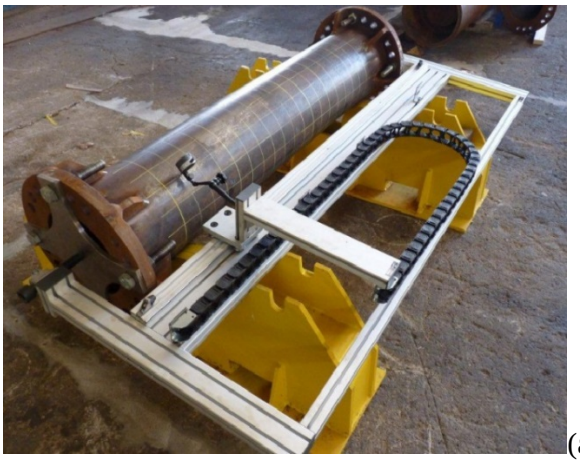
(a)


(b)

**Figure 2**. (a) Device for measuring initial wrinkling of tube wall; (b) Ring specimen extracted from ∅355.6/12 tube after splitting.

The tubular members have been capped with 40-mm-thick circular plates welded to the member ends. Each plate is bolted to a "stiff part", which connect the specimen ends to the hinges of the testing device, as shown in Figure 3. The stiff parts (C1D1 and C2D2) have a length $L_S$ equal to 2.22 m and 1.72 m for the short and long tubular specimens respectively, and remain practically undeformed during the test. Eighteen M30 12.9 bolts are used in the connection of the flange to the stiff part, as shown in Figure 4. The hinges allow rotation about the vertical axis (i.e. rotation on the horizontal plane), but restrict the rotations with respect to the other two axes

(out-of-plane rotations). Under this set-up, the specimen (together with the 2 stiff parts) can be considered as simply-supported in the horizontal plane. In order to stiffen the tube-to-flange connection and avoid local buckling at the two ends of the tubular member, 20-mm-thick stiffeners have been welded around the circumference of the tube Figure 4.

## 2.5 Experimental Results for Tubular Beam- Columns

### *2.5.1 Axial Compression Experiments*

Four axial tests are conducted under pure axial compression on short (1490mm) and long (4490 mm) tubular specimens. The compressive load is applied through the actuator at a constant displacement rate of 1.7mm/min. Twelve strain gauges have been instrumented on circumferential positions through 3 different cross sections, and four LVDTs are used along the axial direction around the circumference of the specimens. The specimen surface has been grid marked as shown in Figure 4 with a 50mm-wide square grid. The test results are depicted in Table 2, in terms of the maximum load $N_{\max}$ sustained by the each specimen.

The buckled geometry of the short specimen AS1 under axial compression is presented in Figure 5a. Local buckling occurred in the form of bulges located near the end section due to stiff end effects. The non-axisymmetric shape of the buckled pattern is attributed to the eccentricity of the tubular specimens end with respect to the line of axial load application. Failure of the long tube specimen AL1, shown in Figure 5b, is due to global buckling (beam buckling). Further increase of axial compression resulted in localized damage at the mid-span in the form of an inward local buckle.

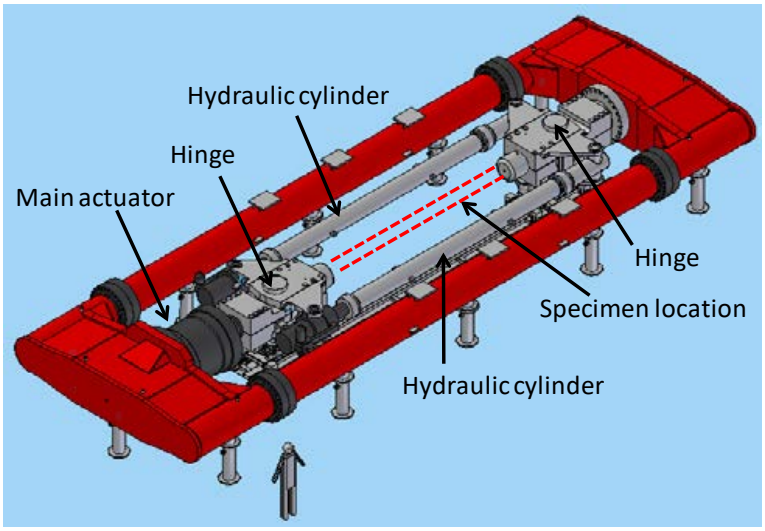


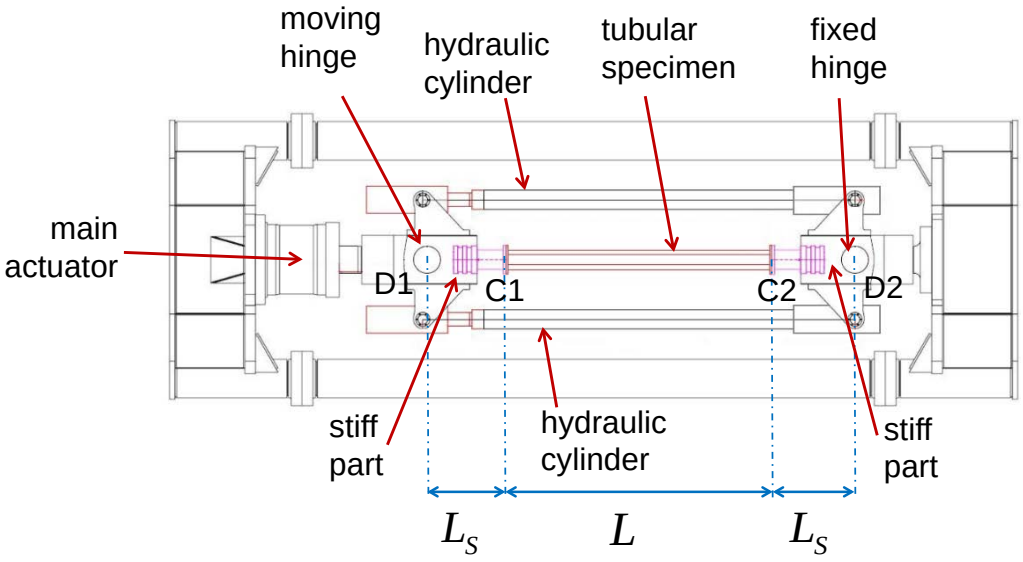


**Figure 3.** Experimental set-up for large scale testing: (a) three-dimensional sketch and (b) plan view.

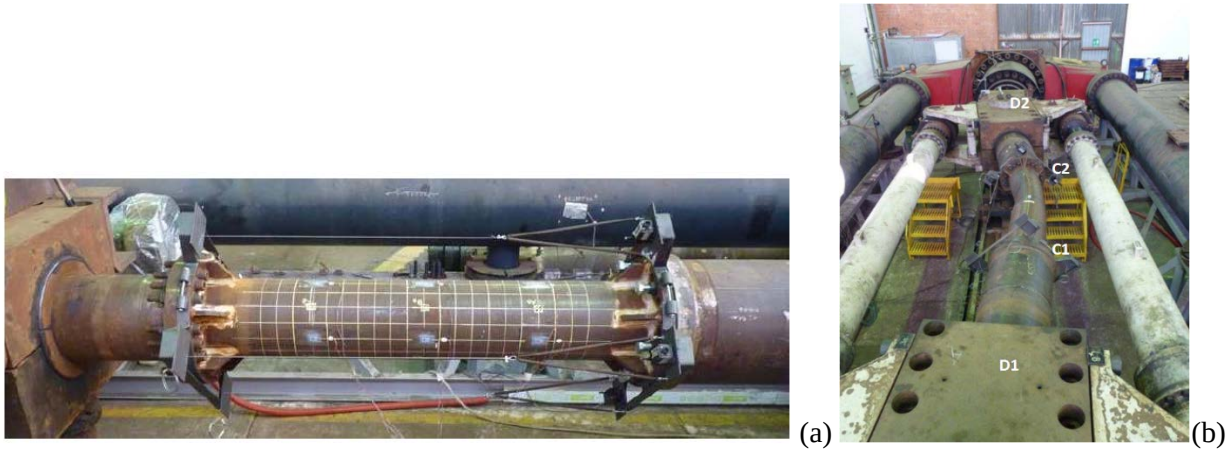


(a) (b)

**Figure 4**. Short column BS-25: (a) in the testing machine before testing and (b) buckled shape after testing.

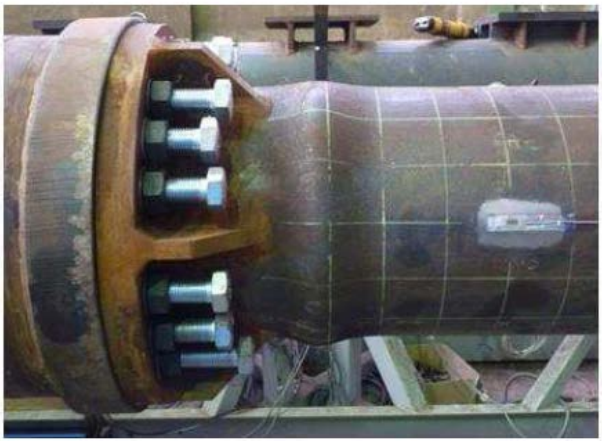

(a)

(b)

**Figure 5**. Axial compression tests: (a) short specimen ASl with local buckling near its end (top); (b) and (c) long specimen AL1 with global buckling (bottom left) followed by local buckling (bottom right).

**Table 2.** Experimental results from axial compression tests.

| Specimen | ID | $N_{max}$ (kN) | $N_{max}/N_y$ | $\delta_{Nmax}$(mm) | $\delta_{Nmax}/L$ |
|---|---|---|---|---|---|
| **Short Column** | **AS1** | 10254 | 1.289 | 10.4 | 0.00697 |
| | **BS1** | 7961 | 1.368 | 8.79 | 0.00589 |
| **Long Column** | **AL1** | 10857 | 1.365 | 18.7 | 0.00390 |
| | **BL1** | 7812 | 1.342 | 17.0 | 0.00361 |

The load-displacement curves for the compression tests are presented in Figure 6. In those curves, the reported displacement is the curve that uses the average of the four LVDT curves. The axial load is normalized by the plastic (yield) axial load $N_y$, computed with the nominal yield stress of the steel material ($\sigma_y = 590$ MPa) and the nominal geometric properties of the cross-section ($N_y = \sigma_y A$). The values of the $N_{\max}/N_y$ ratio are significantly higher than unity, mainly because of the actual value of yield stress, which is significantly higher than the nominal yield stress value.

The experimental results are shown in Table 2 in terms of the maximum load and the corresponding displacement and in Figure 6 in terms of the load-displacement curve. The results show that, for the specific cross-section, the maximum compressive axial load appears to be similar for short and long columns. On the other hand, the normalized deformation capacity is significantly lower in the case of long beam-columns compared with the case of short members.

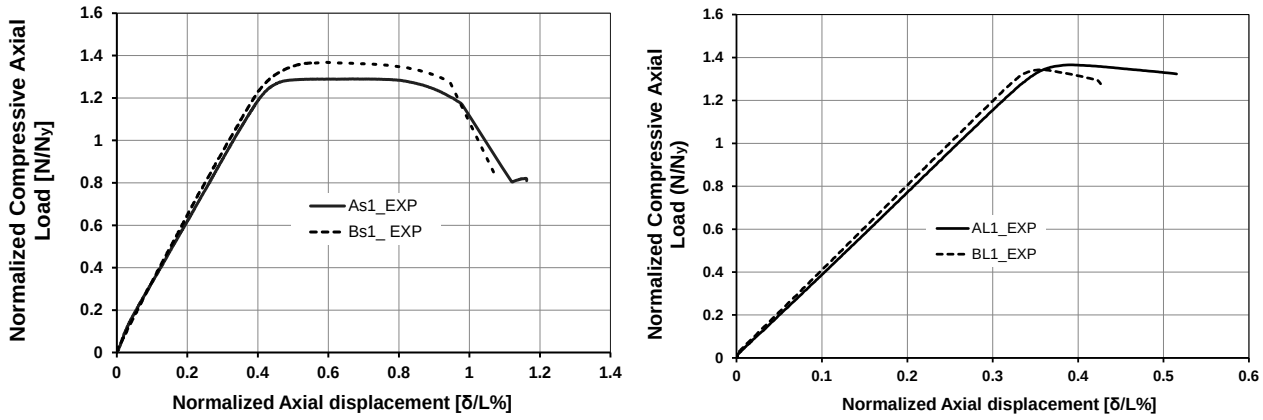


(a) (b)

**Figure 6**. Load-displacement curves for the axial compression tests of (a) short and (b) long specimens.

*2.5.2 Combined Loading Experiments*

Fourteen full scale tests have been performed on short (1850mm) and long (4850 mm) simply-supported tubular specimens of section "A" and "B", under combined loading of axial compression and bending. A "axial load $\rightarrow$ bending" or "$N \rightarrow M$" loading sequence has been employed as follows (see also Table 1); the axial load is increased up to a specific value, which is a percentage (namely 13, 25, 50 and 75%) of the cross-sectional plastic load $N_y$, calculated with the nominal material yield stress (590 MPa). Subsequently, the axial load is held fixed, and the bending is gradually applied until failure occurs, through end rotation-controlled conditions. Four strain gauges have been installed at four circumferential positions around the mid span section. Moreover, two LVDTs have been instrumented to record axial deformation and two LVDTs are used to record the transversal displacement of the specimen. Hinge rotation is also recorded during bending application. The experimental results of the combined axial-bending loading tests for the short specimens are shown in Table 3,

and the buckled shape of a short specimen is shown in Figure 7. A typical buckled shape for short specimens, denoted as "BS", and the corresponding moment-rotation curves are presented in Figure 8. The results in those Figures show that an inward local buckle is developed during the application of bending, at mid-span location of the specimen. It is noted that bending values have been normalized with the value of the yield moment $M_y = \sigma_y W_{el}$, where $W_{el}$ is the elastic bending resistance of the cross-section and $\sigma_y$ is taken equal to 590 MPa. In Table 3 the values of axial force are also normalized with the plastic load of the cross section $N_y^*$, calculated with the actual material yield stress (723 MPa), obtained from the coupon material tests.

The experimental results of the combined loading tests for the long specimens are shown in Table 4 and the moment-rotation curves of the "AL" specimens are depicted in Figure 9. The buckled shape of specimen BL-50 is shown in Figure 10, and similar buckled patterns have been observed in all long specimens; a smooth inward wrinkle is developed at mid-span after reaching the maximum bending moment, resulting in localization of deformation and excessive lateral displacement.

Similar to previous results on short beam-columns, the bending moment capacity in those long beam-columns is significantly decreased with increasing axial compression loading. Moreover, section A specimens have higher bending capacity than section B specimens (in both short and long members) due to their larger cross sectional size.

**Table 3**. Short beam-columns: results from combined loading tests.

| specimen | $N$ (kN) | $N/N_y$ | $N/N_y^*$ | $M_{\max}$ (kNm) | $M_{\max}/M_y$ | end rotation (degrees) |
|---|---|---|---|---|---|---|
| **AS-13** | 1340 | 0.169 | 0.143 | 891 | 1.305 | 2.6 |
| **AS-25** | 2500 | 0.315 | 0.267 | 732 | 1.072 | 1.9 |
| **AS-50** | 5000 | 0.629 | 0.534 | 377 | 0.552 | 1.1 |
| **AS-75** | 7600 | 0.956 | 0.812 | 102 | 0.149 | 0.4 |
| **BS-13** | 1000 | 0.172 | 0.140 | 575 | 1.258 | 2. 4 |
| **BS-25** | 1865 | 0.320 | 0.262 | 492 | 1.076 | 1.8 |
| **BS-50** | 3980 | 0.684 | 0.558 | 209 | 0.457 | 1.0 |
| **BS-75** | 5922 | 1.018 | 0.831 | 76 | 0.166 | 0.5 |

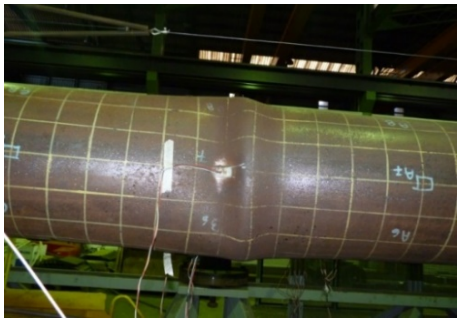
(a)


(b)

**Figure 7**. Buckled specimens under combined loading tests; specimen (a) BS-13 and (b) BS-75.

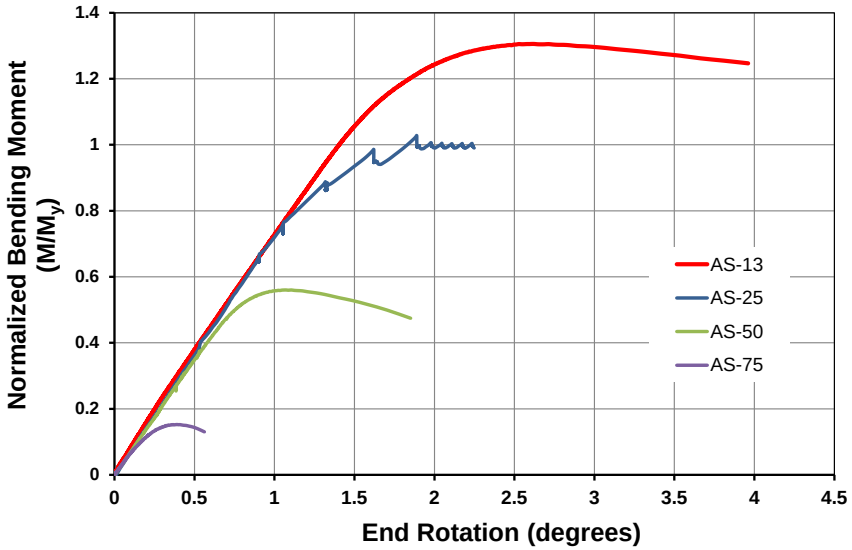


**Figure 8**. Combined loading tests; moment- rotation curves for short columns "AS".

**Table 4**. Long beam-columns: results from combined loading tests.

| specimen | $N$ (kN) | $N/N_y$ | $N/N_y^*$ | $M_{max}$ (kNm) | $M_{max}/M_y$ | end rotation (degrees) |
|---|---|---|---|---|---|---|
| **AL-25** | 1530 | 0.192 | 0.163 | 670 | 0.981 | 4.4 |
| **AL-50** | 2590 | 0.326 | 0.277 | 441 | 0.646 | 3.3 |
| **AL-75** | 4588 | 0.577 | 0.490 | 150 | 0.220 | 1.7 |
| **BL-25** | 1000 | 0.172 | 0.140 | 450 | 0.984 | 4.2 |
| **BL-50** | 2020 | 0.347 | 0.283 | 232 | 0.507 | 3.0 |
| **BL-75** | 3298 | 0.566 | 0.463 | 79 | 0.173 | 1.5 |

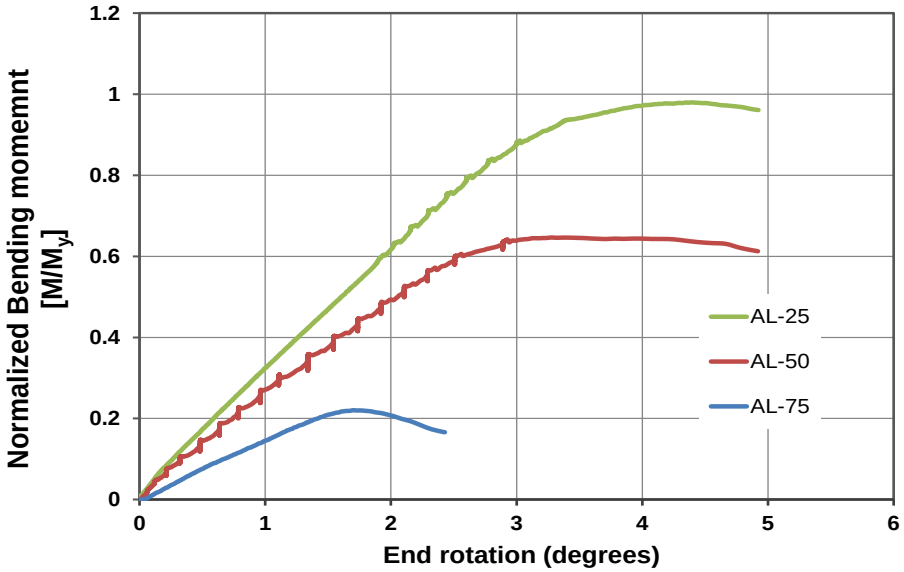


**Figure 9**. Combined loading tests on long columns; moment-rotation curves.

**Figure 10**. Beam-column BL-50 after testing

## 3. NUMERICAL SIMULATION OF TESTS

The tests described in the previous section are simulated with finite element models. The comparison of numerical and experimental results is aimed at calibrating the finite element models, to be used in extensive parametric studies, to be presented in a later section of the paper.

The finite element models are developed in ABAQUS/Standard, and are capable of describing large displacements and local buckling of the tubular members, as well as plastic deformations of the steel material through a $J_2$ (von Mises) flow constitutive model. The tube is simulated with four-node reduced-integration shell elements (S4R). The tubes have been modelled with uniform thickness equal to 12.49 mm and 10.26 mm, which are the measured average values for sections A and B respectively.

Initial geometric imperfections in the numerical model are considered in the form of initial wrinkles along the tubular member. Towards this purpose, an eigenvalue analysis of the tubular member is conducted under pure bending loading conditions, and the corresponding first buckling mode is scaled through an appropriate factor that multiplies the mode displacements to achieve a targeted value of initial wrinkling imperfection amplitude. The values of this amplitude have been considered quite small, equal to 2.6% of tube wall thickness, which is a representative value from the relevant wrinkling measurements as reported in the previous section of the present paper, also reported in [30]. The scaled buckling shape is superimposed to the initial perfect geometry of the tube, so that the initial nodal coordinates represent the initially wrinkled pattern of the tubular member. Furthermore, residual (initial) stresses in hoop direction have been considered as initial stresses of the model in the form of a linear distribution through the tube thickness with a maximum value of 122 MPa, according to measurements [30]. Residual stresses in the longitudinal direction have been measured quite small and are neglected in the numerical model.

The stiff parts, which connect the tubular specimen ends to the machine hinges, are simulated as rigid members using beam elements of very large bending and axial stiffness. The shape of the buckle may not always be symmetric with respect to both the middle-section and the plane of bending, therefore, the entire tube is simulated, without any symmetry considerations.

In the case of combined axial/bending conditions, the analysis follows a loading sequence in accordance with the experimental procedure; axial compressive load is applied first up to a prescribed level and, subsequently, keeping the axial load constant, bending is applied gradually using a Riks algorithm. Soon after the maximum bending moment is reached, local buckling initiates, and continuation of bending in the post-buckling range results in the development of a sharp local buckle (kink). Comparison of the buckled shapes obtained numerically with the buckled shapes observed in the experiments is also conducted.

For consistency with the experimental set-up shown in Figure 3, in the numerical models, the end sections of the tubular models (sections C1 and C2) are connected to the stiff tubular segments through a “kinematic coupling” constraint, which relates the degrees of freedom of the shell nodes at the end section with the degrees of freedom of a fictitious node, referred to as the “reference node”. The latter node is located at the centroid of the end section. This kinematic "constraint" simulates the bolted connection of each specimen end with the corresponding stiff end part. The entire specimen model is considered simply-supported at both ends of the rigid segments D1 and D2. The model configuration is shown in Figure 11.

For the case of axial compression, the numerical and experimental results are compared in Figure 12, in terms of load-displacement curves for the short specimen “AS1”. This specimen exhibited a bulging buckle near the end section of the tubular specimen. On the other hand, the buckling failure of AL1 model is shown in Figure 13, which correlates well with the shape depicted in Figure 10.

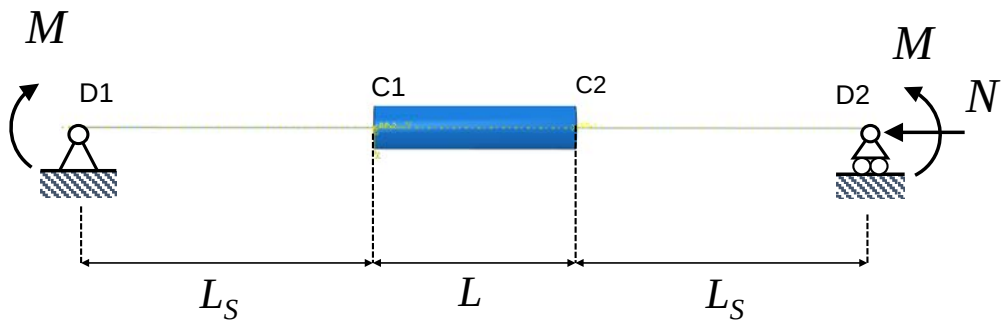


**Figure 11**. Schematic configuration of the test set-up (sketch is for short specimens, similar set-up is used for long specimens).

For the case of combined loading, the finite element predictions are compared with the experimental data in terms of the thrust-bending interaction curves in Figure 14. The comparison shows that the numerical models provide very good predictions of the ultimate capacity of the steel tubular beam-columns under consideration. Furthermore, the buckled shapes of the specimens obtained numerically as shown in Figure 15 compare very well with the corresponding buckled shapes observed in the combined loading tests (Figure 7a, Figure 7b and Figure 10).

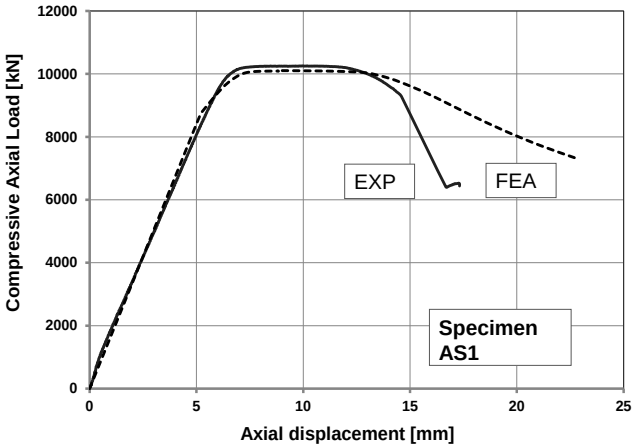


**Figure 12**. Load-displacement curve for AS1 specimen in comparison with FE analysis results.

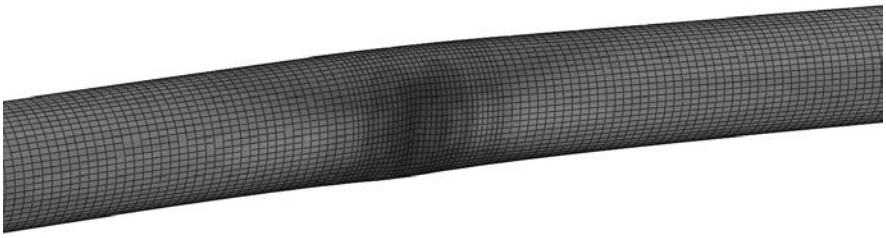

**Figure 13**. Detail of local buckle axial compression for AL1 specimen simulation.

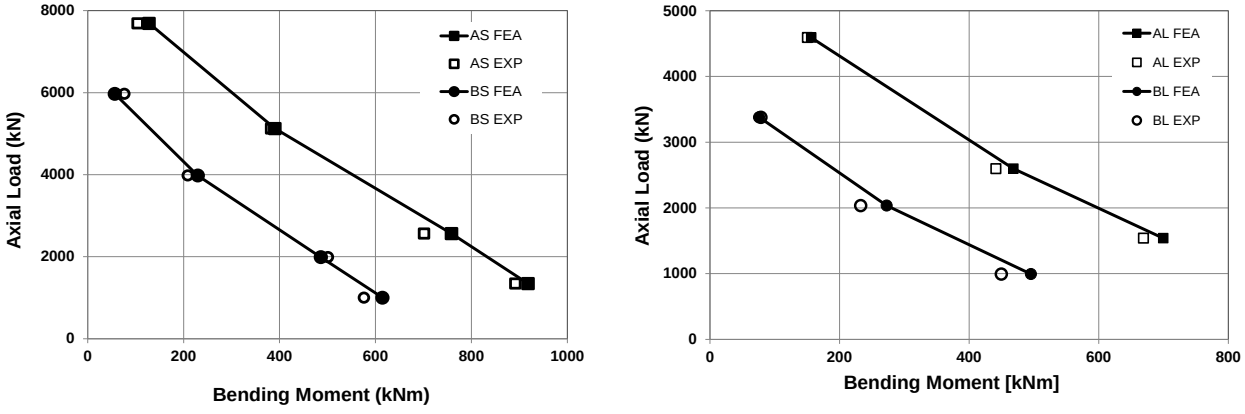


(a) (b)

**Figure 14**. Comparison of test results (EXP) and finite element predictions (FEA); (a) short specimens AS and BS and (b) long specimens AL and BL.

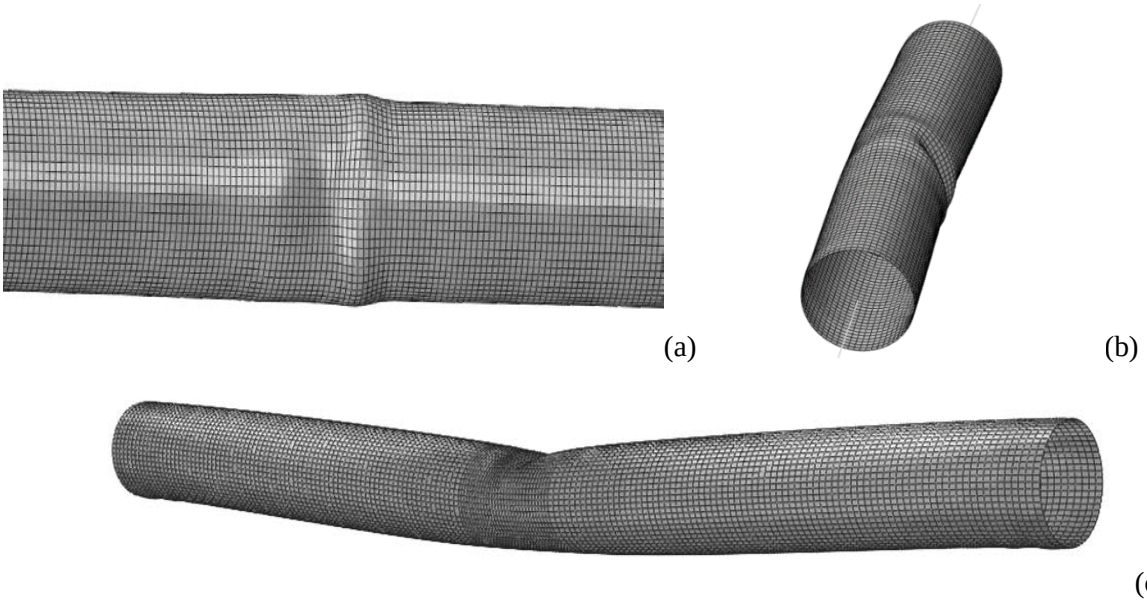


**Figure 15**. Buckled shapes for (a) AS-75, (b) BS-75 and (c) BL-75 obtained from the numerical models.

## 4. NUMERICAL PARAMETRIC STUDY

Apart from the simulation of the experimental procedure, finite element simulations have also been performed to examine the cross-sectional capacity of high strength steel tubular members, as well as to obtain appropriate buckling curves and interaction diagrams of axial compression and bending. In the present parametric study, two types of cross-sections have been considered, denoted as "AA" and "AB", as presented in Table 5. The length $L$ of the tubular member has been considered between 1 m and 14 m, covering a wide range of slenderness values. The tubular members are assumed simply-supported at the two ends. Despite the fact that length values equal to 14 m for those tubes may not be very realistic for typical structural applications, they have been considered in the present analysis for the sake of tracing the buckling curves for global buckling within the elastic buckling range. The material stress-strain curve used in the parametric analysis is considered as bilinear with yield stress equal to 590 MPa. The post-yield hardening modulus is equal to $E/500$, which is very close to the hardening modulus observed in the coupon tests of the high strength steel material. The numerical results, obtained in the present parametric study, are compared with the design provisions of European specification EN 1993, as well as those of American Standards AISC-LRFD and API 2A-LRFD.

**Table 5**. Geometric and mechanical properties of tubular sections used in the parametric study.

| **Section** | Outer Diameter $D$ (mm) | Thickness $t$ (mm) | $D_0 / t$ | $\sigma_y$ (MPa) | **Class*** |
|---|---|---|---|---|---|
| **AA** | 355.6 | 8 | 44.5 | 590 | 4 |
| **AB** | 355.6 | 12.5 | 28.5 | 590 | 3 |

**According to EN-1993-1-1 classification.*

According to EN 1993-1-1, cross section AA is classified as class 4 and therefore, to obtain the corresponding cross-sectional strength considering local buckling phenomena, $\sigma_{xRk}$ , the provisions of EN 1993-1-6 have been used. In this case, the value of $\sigma_{xRk}$ replaces the yield stress $\sigma_y$ in the design equations in sections 6.2 and 6.3 of EN 1993. Furthermore, because of the very small values of initial wrinkles measured prior to testing (less than 2.6% as described in paragraph 2.3), excellent fabrication conditions have been assumed, so that the quality factor $Q$ defined in Annex D (Table D1) of EN1993-1-6 is taken equal to 40.

### 4.1 Cross-sectional behavior and initial wrinkling sensitivity

The first part of the parametric study is aimed at examining the axial and bending strength of tubular cross-sections, in an attempt to evaluate the current EN1993-1-1 provisions for cross-section classification of high-strength steel CHS members. The failure mode that governs cross-sectional strength is local buckling of tube wall in the form of wrinkles, due to excessive compression, a shell-type mode. Herein, local buckling under both axial and bending loads is examined, computing the ultimate load of the cylinder under consideration in terms of wrinkling imperfection.

To perform those analyses, an eigen-value analysis of a perfect elastic tubular member under bending is conducted first, to obtain the corresponding buckling mode for the initial imperfection shape, as described in section 3. This buckling mode is characterized by non–axisymmetric wrinkles along the compression side of the tube with increasing amplitude from the capped ends to mid-span. The corresponding initial wrinkling pattern of the finite element model is shown in Figure 16. Finer mesh is employed in the mid-span of the tubular member in order to describe accurately the deformation of the critical region of the buckle (Figure 16), whereas coarser mesh is used in the regions of the tubular member away from the mid-span. The element size in the longitudinal direction within this 500-mm-long central region is equal to 1/10 of the half-wave length of the wrinkle. Upon definition of the imperfect initial geometry of the cylinder, non- linear finite element analysis is conducted to calculate its structural behavior and the buckling strength of the tubular member under axial and bending loading.

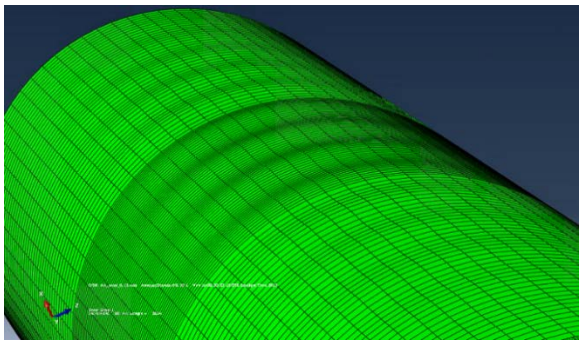

**Figure 16**. The detailed geometry of a wrinkled model with $w_0/t = 0.15$.

*4.1.1 Axial Compression*

Initially wrinkled tubular members ∅355.6/8 (AA section) and ∅355.6/12.5 (AB section) are considered with various wrinkling amplitudes, subjected to axial compressive loading. The tubular members employed are quite short (2000 mm) to exclude any effects of global (Euler-type) buckling. The corresponding axial load-displacement curves are presented in Figure 17, where the load values are normalized by the plastic axial force value $N_y$ calculated equal to 5154 kN and 7949 kN for AA and AB sections, respectively, considering a yield stress of 590 MPa. The buckling strength of tubes AA and AB is shown with respect to wrinkling amplitude in Figure 18, whereas, the failure mode of AA tubular members for wrinkling amplitude equal to 6% is shown in Figure 19. The results show that those members are capable of reaching the plastic thrust level $N_y$ for wrinkling amplitude equal to 20% of wall thickness.

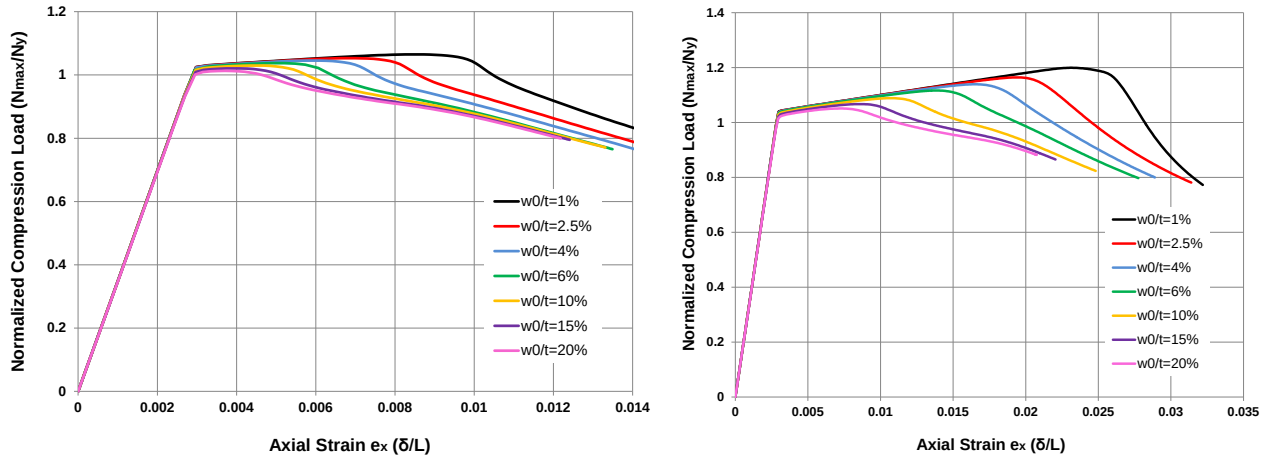


(a) (b)

**Figure 17**. Load vs displacement curves for (a) AA and (b) AB; 2m-long tubular members with various wrinkling amplitudes ( $w_0/t$ ) under axial compression.

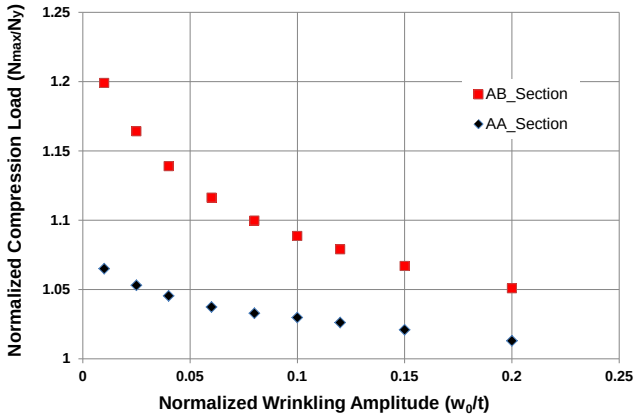


**Figure 18**. Normalized axial compression capacity in terms of wrinkling amplitude ( $w_0/t$ ) for AA and AB sections.

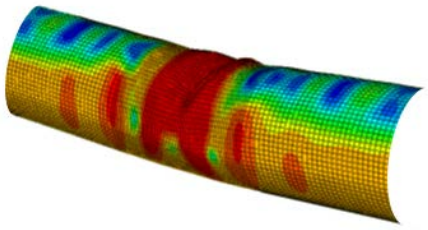

**Figure 19**. Failure mode for AA member under axial compression; initial wrinkling imperfection amplitude $w_0/t =$ 6%.

*4.1.2. Bending*

Initially-wrinkled short-length tubular members with cross-sections ∅355.6/8 (section AA) and ∅355.6/12 (section AB) are subjected to bending loading. The corresponding moment-curvature diagrams are presented in Figure 20 for various wrinkling amplitudes. In these diagrams the moment values have been normalized by the value of the yield moment $M_y$. The value of $M_y$ is equal to 448.14 kNm and 662.76 kNm for AA and AB cross-sections, respectively, considering the yield stress value of 590 MPa. The global curvature $k$ obtained from the finite element analysis is calculated as $k = \varphi / L$, where $\varphi$ is the total relative rotation of the two end sections and $L$ is the distance between the two end sections. The value of $k$ has been normalized with the nominal value of yield curvature ($k_y$), calculated as $k_y = M_y / EI$, where $EI$ is the bending rigidity of the tubular cross-section. The value of $k_y$ is equal to 1.69×10$^{-5}$ mm$^{-1}$ and 1.719×10$^{-5}$ mm$^{-1}$ for AA and AB cross-sections, respectively. The maximum bending strength $M_{\max}$ and the corresponding global curvature of the tubes, denoted as $k_{\max}$, has been plotted in terms of wrinkling amplitude in Figure 21 and Figure 22, respectively and the failure modes of the tubular models are shown in Figure 23 and Figure 24 for various wrinkling amplitudes.

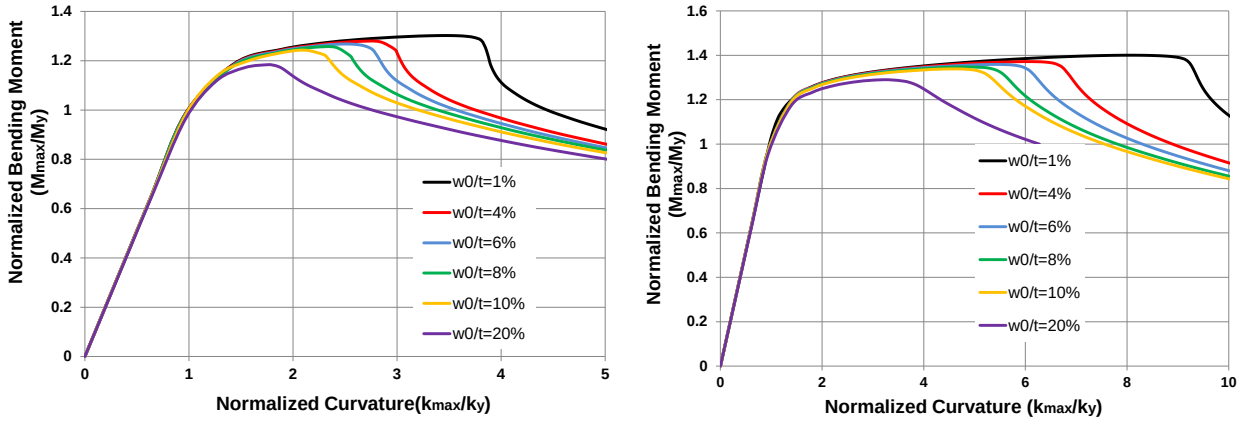


(a) (b)

**Figure 20**. Moment - curvature diagrams for (a) AA and (b) AB sections under pure bending loading for wrinkling amplitudes ($w_0/t$) between 1% and 20%.

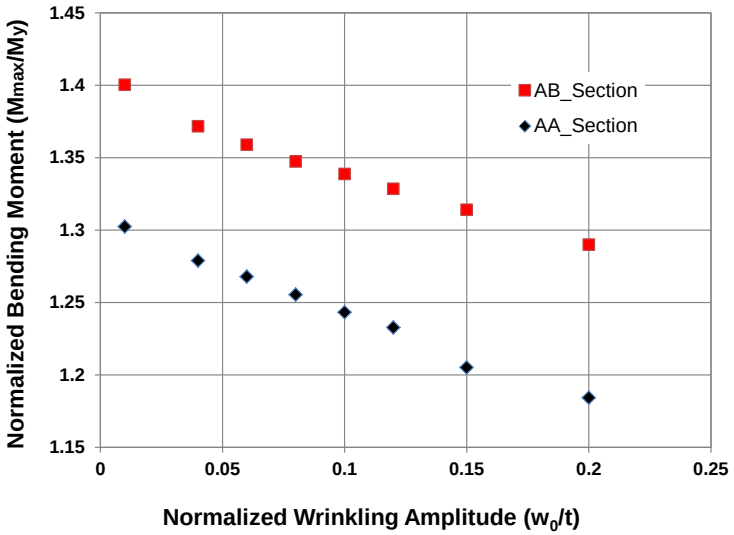


**Figure 21**. Normalized maximum bending moment in terms of normalized wrinkling amplitude curves for AA and AB sections.

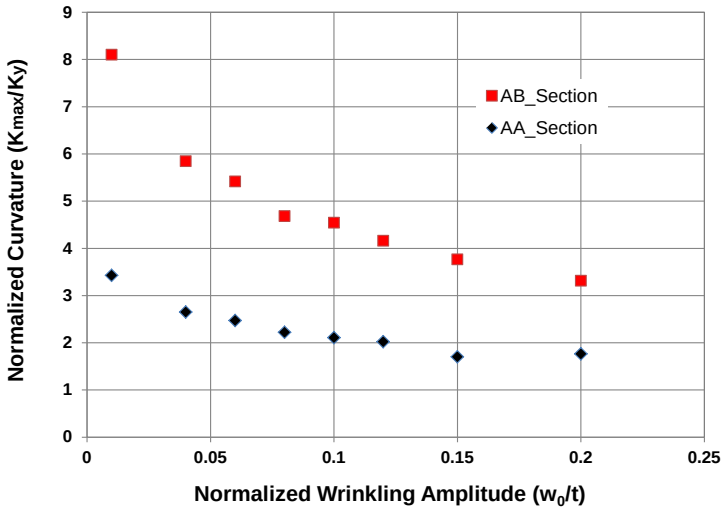


**Figure 22**. Maximum curvature vs normalized wrinkling amplitude curves for AA and AB tubular models.

The results in Figure 21 and Figure 22 indicate that the ∅355.6/8 section (AA) is capable of sustaining significant load and deformation beyond first yield of the cross-section, despite the fact that, according to EN1993-1-1, this section is classified as class 4. In particular, the maximum bending strength ($M_{\max}$) is significantly higher than the bending moment $M_y$ for the range of initial wrinkling amplitudes under consideration. For values of normalized initial imperfection ($w_0/t$) less than 8%, the maximum bending moment is 25% higher than $M_y$, whereas for $w_0/t$ less than 5% (a reasonable value for seamless tubes), the fully-plastic moment $M_P$ is exceeded ($M_P = 1.27M_y$), indicating a Class 2 section. In addition, the

corresponding curvature is higher than twice the value of $k_y$ for $w_0/t$ greater than 10%. These results indicate that the current EN 1993-1-1 classification is quite conservative, penalizing severely the tubular cross-section capacity and resulting in a non-economical design.

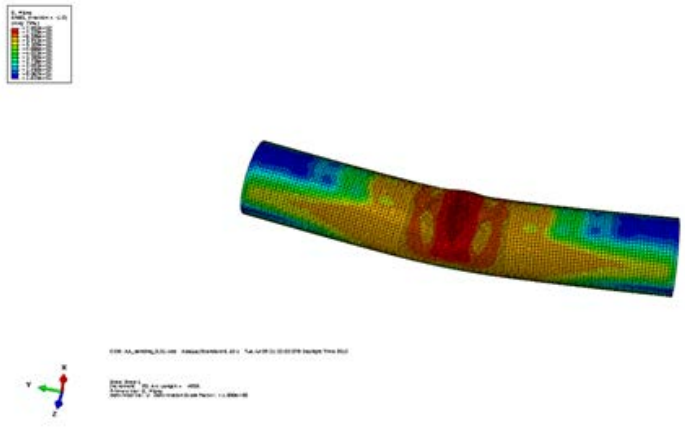

**Figure 23**. Typical failure of short AA column with imperfection $w_0/t = 1\%$ under bending moment.

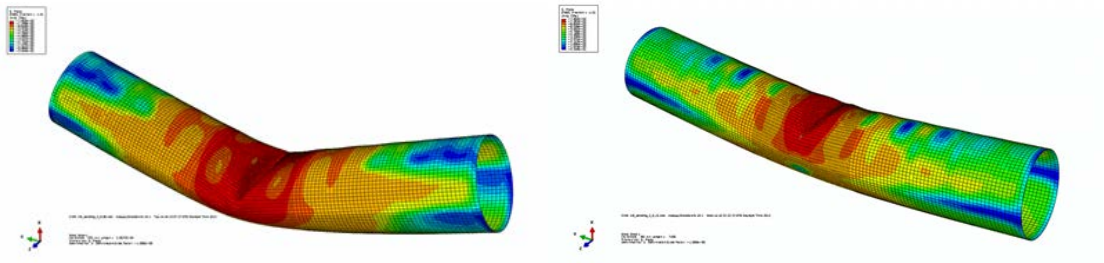

(a) (b)

**Figure 24**. Failure mode of AB tubular members under pure bending with wrinkling amplitude $w_0/t$ equal to (a) 4% and (b) 15%.

### 4.2 Beam-column stability curves

In most design specifications, the global buckling resistance ( $N_u$ ) of structural members under axial compressive loading is given in terms of their column flexural slenderness can be expressed as follows:

$$N_u = \chi \sigma_y A \qquad (2)$$

where $\chi$ is the buckling reduction factor, a function of the column flexural slenderness $\lambda_c$, and $\sigma_y A = N_y$ is the cross sectional plastic resistance of the member.

Using the present numerical tools, the buckling strength under axial compressive load of tubular members with the sections AA and AB and the corresponding reduction factor $\chi$ is calculated, in terms of their slenderness and comparisons are made with the provisions of various design specifications. Measured values of

initial imperfections and residual stresses as described in paragraph 2.3 are taken into account. The wrinkling amplitude is considered equal to 2.6% of the tube thickness, and the residual stresses have a maximum value of ±122 MPa, linearly distributed over the tube thickness. Finally, despite the fact that initial measurements on the tubular specimens showed that their initial out-of-straightness is negligible, a bow-type initial out-of-straightness with amplitude equal to $L/750$ is assumed, which corresponds to the maximum allowed value according to EN 1090-2 [31].

The ultimate buckling load $N_u$ obtained numerically for the two cross sections under consideration, namely AA and AB, for several tube lengths corresponding to wide range of flexural slenderness $\lambda_c$ is depicted in Figure 25 and Figure 26 in the form of stability curves. The buckling load is normalized by the normal plastic load $N_y = A\sigma_y$. The stability curves are compared with the provisions of EN 1993, API RP-2A and AISC-LRFD.

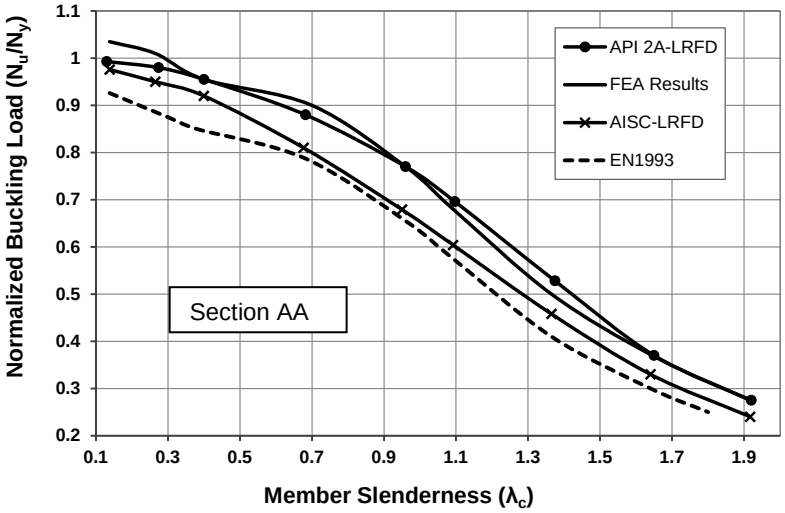


**Figure 25**. Stability curve for section AA from finite element analysis, compared with EN 1993 and American standards.

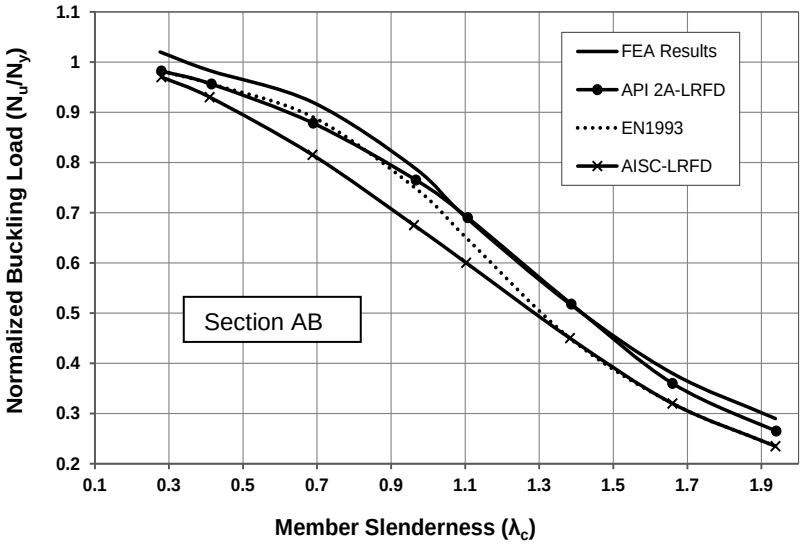


**Figure 26**. Stability curve for section AB from finite element analysis, compared with EN 1993 and American standards.

The numerical results in Figure 25, indicate that EN 1993 predictions are conservative for section AA. The results are well correlated with the stability curve proposed by API standard, while the AISC provisions provide conservative predictions by over 20% for all slenderness values. The stability curves of section AB, compare reasonably well with the EN 1993 and API predictions. For large values of column slenderness ($\lambda_c \geq 1$) EN 1993 underestimates the buckling strength by approximately 10%. On the other hand, for intermediate values of slenderness, the AISC standard underestimates the axial buckling strength by about 10%. Buckled shapes due to axial compression for short and long members with section AA are depicted in Figure 27.

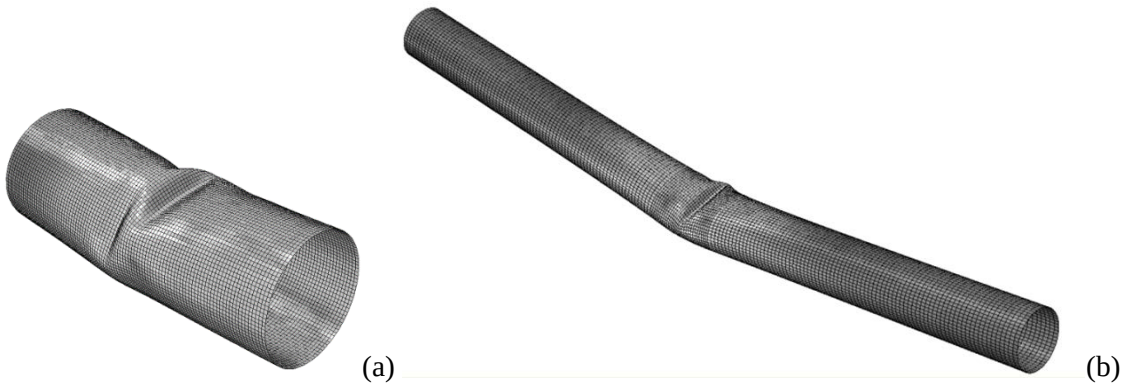


**Figure 27**. (a) Buckled shape of 1-meter-long (stub) tube of section AA under axial compression ($\lambda_c$=0.13), exhibiting shell-type buckling instability; (b) Buckled shape of 5-meters-long tube of section AA under axial compression ($\lambda_c$=0.69), exhibiting a combination of Euler-type and shell-type buckling instability.

In non-slender members ($0.1 \le \lambda_c \le 0.3$), local buckling governs the response. Upon initial wrinkling, plastic deformation is accumulated at one wrinkle of the tube wall leading to the development of local buckling. For moderate and large values of flexural slenderness, the tubular member exhibits global (flexural) buckling, and deflects laterally by a substantial amount. Subsequently, following this global deflection, local buckling of the tube wall occurs at mid-span.

### 4.3 Thrust-bending interaction diagrams

Figure 28 and Figure 29 present interaction diagrams for the combined action of axial and bending ($N \rightarrow M$ loading sequence), for 5m-long and 8m-long members with sections AA and AB, subjected to combined loading. The corresponding values of slenderness are 0.769 and 1.230 for section AA members and 0.759 and 1.215 for section AB members. These diagrams show the significant reduction of bending moment resistance of the member $M_u$ with increasing level of axial compressive force. The reported values of moment correspond to the moment applied at the two ends of the tubular beam-column. Clearly, the maximum bending moment occurs at mid-span of the tube, due to the second order $P-\delta$ effect. Similar geometrical and material properties are employed with the previous analysis (Sections 4.1 and 4.2) for tubes with AA and AB sections. Initial wrinkling imperfections, out-of-straightness and residual stresses, are assumed similar to the ones employed in the previous section for column stability analysis (Section 4.2).

The axial force-moment interaction diagrams ($N_u, M_u$) obtained numerically are compared with the curves proposed by design specifications as shown in Figure 28 and Figure 29. The axial load and bending moment values are normalized by the values of plastic (yield) thrust $N_y = A\sigma_y$ and the yield moment $M_y$ of the cross-section. EN 1993 provisions are employed with the beam-column Method 1, described in the relevant Annex A of EN 1993-1-1. Those provisions underestimate the bending capacity of the tubular member by approximately 35% for both AA and AB sections. This conservativeness is attributed to the fact that the CHS members under consideration are classified as class 4 and 3, respectively. However, the test results presented in section 2, as well as the present numerical results, indicate that these sections can sustain significant inelastic deformation before reaching their bending moment resistance. The numerical results also show that the AISC provisions penalize the bending strength by over 15%, whereas API RP 2A underestimates the maximum bending moment by approximately 18%. Finally, representative buckled shapes obtained from the finite element models AA and AB are shown in Figure 30.

The comparison between numerical results and specification provisions indicates that the design standards under consideration are rather conservative in predicting the beam-column behavior of CHS members made of high-strength steel. The conservativeness of EN 1993 predictions are mainly due to the "penalizing" classification of CHS cross sections in EN 1993-1-1 demonstrated in section 4.1, a conclusion also reported in [30]. It is the authors' opinion that re-examination of cross-sectional classification for high-strength steel tubes, would result in a more reliable design of tubular members.

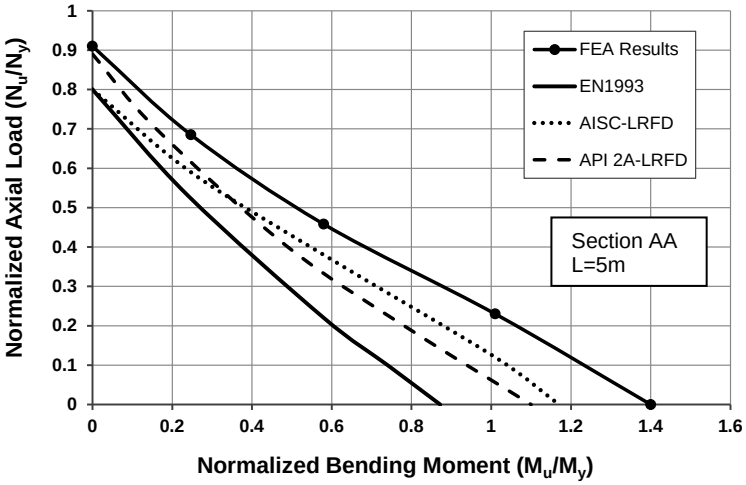


(a)

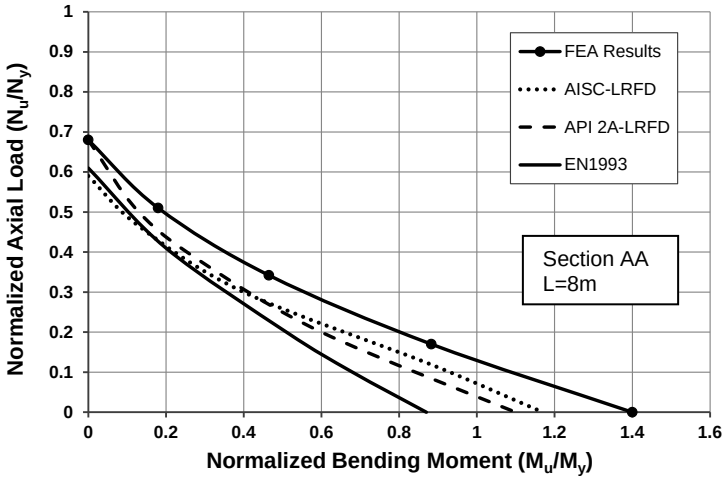


(b)

**Figure 28**. Thrust-bending interaction diagrams for beam-columns with AA section, compared with relevant design standard provisions ( $N \rightarrow M$ loading sequence).

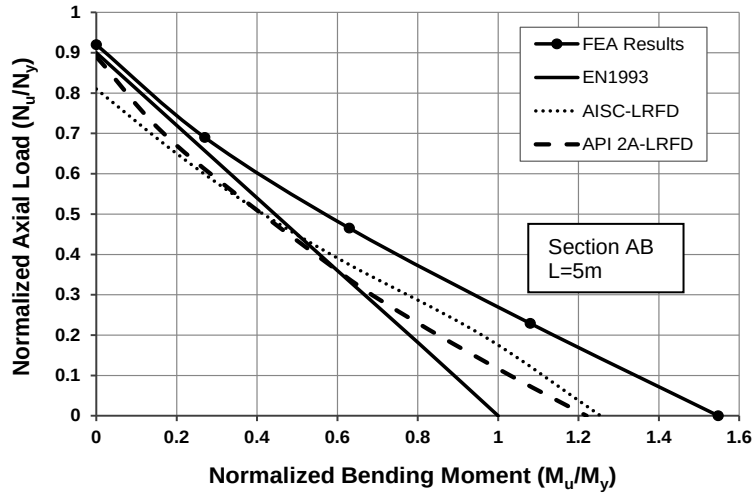


(a)

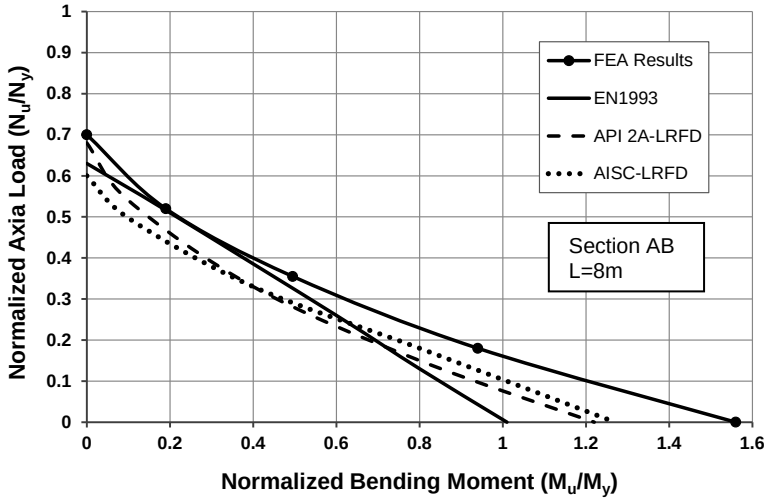


(b)

**Figure 29**. Thrust-bending interaction diagrams for beam-columns with AB section, compared with relevant design standard provisions ( $N \rightarrow M$ loading sequence).

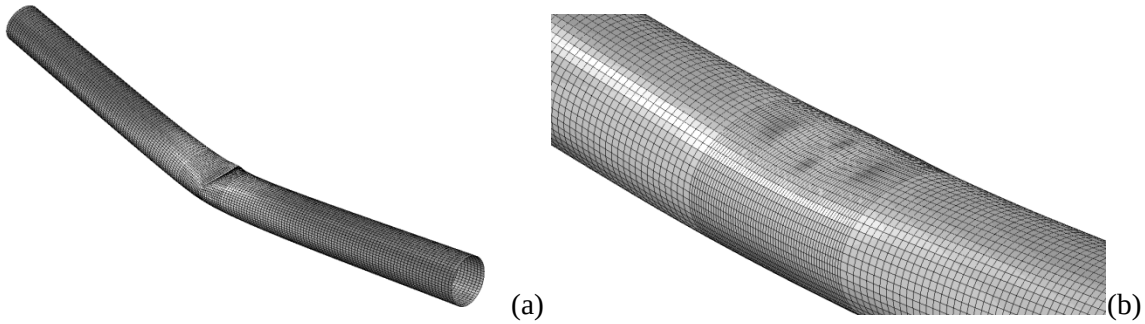

(a) (b)

**Figure 30**. Buckled shapes of (a) 5m-long tube with section AB and (b) 8m-long model with section AA under combined compression and bending.

## 5. CONCLUSIONS AND RECOMMENDATIONS

A combined experimental and numerical investigation has been described in this paper, for determining the ultimate strength of CHS seamless members made of high-strength steel with nominal grade 590. Eighteen full-scale tests have been performed, on short and slender seamless tubular specimens of high-strength steel. Using advanced numerical tools the behavior CHS beam-column has been simulated, and compared with current design practice. The numerical models have been successfully predicted the behavior of pipe specimens under axial and bending loading, in comparison with experimental results. Furthermore an extensive numerical parametric study has been performed on tubular members in order to investigate the effect of wrinkling imperfection on the structural capacity of tubular members. It has been shown that wrinkling imperfection affects the limit bending and axial load values before buckling formation. Moreover stability curves and interaction diagrams have been obtained and compared with the current provisions. It has been concluded that stability curves proposed by EN 1993, API RP 2A, provide reasonable yet conservative predictions for design. On the other hand, AISC provisions for CHS beam-columns appear to be somewhat closer to the numerical results. The EN 1993 provisions penalize the buckling capacity of high-strength steel CHS members of relatively small thickness, mainly because their classification as class 4. This implies that the current EN 1993 classification should be re-examined for high-strength steel CHS sections. Because of this conservative classification, the thrust-bending interaction curves for high-strength steel CHS members obtained by the finite element analyses have indicated significantly higher ultimate capacity with respect to the predictions of the design rules of the above specifications, especially the ones from the EN 1993 provisions.

## ACKNOWLEDGEMENTS

The present work has been supported by the European Commission through the Research Fund for Coal and Steel, ATTEL project: “Performance-Based Approaches for High Strength Steel Tubular Columns and Connections under Earthquake and Fire Loadings”, Grant No. RFSR-CT-2008-00037. The high-strength steel tubular specimens have been manufactured by Tenaris Dalmine S.p.A. The authors would like to thank all partners of the ATTEL project for their useful input and comments throughout this research effort.

## REFERENCES

[1] Rasmussen, G. J. and Hancock, K. (1995). “Test of High Strength Steel Columns”, *Journal of Constructional Steel Research*, Vol. 34, pp. 27-52.

[2] Beg, H. (1996). “Slenderness limit of Class 3 I cross-sections made of high strength steel”, *Journal of Constructional Steel Research*, Vol. 38, No. 3, pp. 201-217.

[3] Sivakumaran, K. S. and Bing, Y. (1998). “Slenderness limit and ductility of high strength steel sections”, *Journal of Constructional Steel Research*, Vol. 46, No. 1, pp. 149-151.

[4] Johansson, B. & Collin, P. (1999). “High strength steel - the construction material of the future”, *International Conference: Steel and Composite Structures*, Delft, The Netherlands.

[5] Shi, G., Ban, H., Bijlaard, F. S. K. (2012). “Tests and numerical study of ultra-high strength steel columns

with end restraints", *Journal of Constructional Steel Research*, Vol. 70, pp. 236–247.

[6] Sherman, D. R. (1976). "Tests of circular steel tubes in bending", *ASCE J. Structural Division*, Vol. 102, pp. 2181-2195

[7] Korol, R. M. (1979). "Critical buckling strains of round tubes in flexure", *International Journal of Mechanical Sciences*, Vol. 21, pp. 719-730.

[8] Chen, W. F. and Ross, D. A. (1977). "Test of fabricated tubular columns", *ASCE J. Structural Division*, Vol. 103, No. 3, pp. 619–34.

[9] Prion, H. G. L. and Birkemoe, P. C. (1992), "Beam-column behavior of fabricated steel tubular members", *ASCE Journal of Structural Division*, Vol. 118, No. 5, pp. 1213–1232.

[10] Elchalakani, M., Zhao, X.-L., Grzebieta, R. (2002). "Bending tests to determine slenderness limits for cold-formed circular hollow sections", *Journal of Constructional Steel Research*, Vol. 58, No. 11, pp. 1407–1430.

[11] Miller, C. D. (1982). "Summary of Buckling Tests on Fabricated Steel Cylindrical Shells in the USA", *Buckling of Shells in Offshore Structures*, ed. Harding, J. E., Dowling, P. J. and Angelidis, C. M., Granada, London, pp. 429-472.

[12] Kulak, G. L. (1996). "Tubular members – large and small", *Engineering Structures*, Vol. 18, pp. 745-751.

[13] Dorey, A. B., Murray, D. W., Cheng, J. J. R. (2000). "An experimental evaluation of critical buckling strain criteria", *International Pipeline Conference*, Calgary, Alberta, Canada.

[14] Reddy, B. D. (1979). "An experimental study of the plastic buckling of circular cylinders in pure bending", *International Journal of Solids Structures*, Vol. 15, pp. 669–683.

[15] Kyriakides, S. and Ju, G. T. (1992). "Bifurcation and localization instabilities in cylindrical shells under bending – Part I: Experiments", *International Journal of Solids Structures*, Vol. 29, No. 9, pp. 1117–1142.

[16] Gresnigt, A. M. and Van Foeken, R. J., (2001). "Local buckling of UOE and seamless steel pipes", *Proceedings of the International Offshore and Polar Engineering Conference* (ISOPE), Stavanger, Norway.

[17] Toma, S. and Chen, W. F. (1979). "Analysis of fabricated tubular columns", *ASCE Journal of Structural Division*, Vol. 105, No. 11, pp. 2343–2366.

[18] Sohal, I. S., and Chen, W. F. (1988). "Local and Post-Buckling Behavior of Tubular Beam-Columns", *ASCE Journal of Structural Engineering*, Vol. 114, No. 5, pp. 1073–1090.

[19] Wagner, A. L., Mueller, W. H. and Erzurmlu, H. (1976). "Design interaction curve for tubular steel beam-columns", *Offshore Technology Conference*, OTC Paper No. 2684, pp. 755 – 764.

[20] Karamanos, S. A. and Tassoulas, J. L. (1992). "Tubular Members II: Local Buckling and Experimental Verification.", *ASCE Journal of Engineering Mechanics*, Vol. 122, No. 1, pp.72-78.

[21] Jiao H. and Zhao X.-L. (2003). "Imperfection, residual stress and yield slenderness limit of very high strength (VHS) circular steel tubes", *Journal of Constructional Steel Research*, Volume 59, Number 2, pp. 233-249.

[22] Jiao, H. and Zhao, X. L. (2004). "Section slenderness limits of very high strength circular steel tubes in bending", *Thin-Walled Structures*, Vol. 42, pp. 1257–1271.

[23] European Committee for Standardization (2005). *Eurocode 3: Design of steel structures. Part 1-1: General rules and rules for buildings*, CEN EN 1993-1-1, Brussels.

[24] European Committee for Standardization (2007). *Eurocode 3: Design of steel structures. Part 1-6: Strength and Stability of Shell Structures*, CEN EN 1993-1-6, Brussels.

[25] European Committee for Standardization (2006). *Eurocode 3: Design of steel structures. Part 1-12: Additional rules for the extension of EN 1993 up to steel grades S700*, CEN EN 1993-1-12, Brussels.

[26] American Institute of Steel Construction (2000). *Load Resistance Factor Design Specification for steel hollow structural sections*, AISC-LRFD, Chicago, Illinois.

[27] American Petroleum Institute (1993). *Recommended Practice, Designing and Constructing Fixed Offshore Platforms – Load and Resistance Factor Design*. Recommended practice 2A-LRFD, 1st Edition. Washington, DC.

[28] Comité International pour le Dévelopment et l' Etude de la Construction Tubulaire (1992). *Structural Stability with Hollow Sections*. CIDECT design guide No. 2, Springer-Verlag.

[29] Jaspart, J.-P. *et al*., (2012). *Performance-based approaches for high strength tubular columns and connections under earthquake and fire loadings*, project ATTEL final report, RFCS, European Commission, Brussels, Belgium (http://bookshop.europa.eu/).

[30] Pappa, P. and Karamanos, S. A. (2012). "Buckling of High-Strength Steel CHS Tubular Members Under Axial Compression and Bending", *14th International Symposium on Tubular Structures*, Paper No. 104, London, UK.

[31] European Committee for Standardization (2007). *Technical requirements for the execution of steel structures*, CEN EN 1090-2, Brussels.

[32] Boissonnade, N., Jaspart, J.-P., Muzeau, J.-P., Villette, M. (2004), "New interaction formulae for beam-columns in Eurocode 3: The French–Belgian approach", *Journal of Constructional Steel Research*, Vol. 60, pp. 421–431.